Sum rule distortions in fluorescence-yield x-ray magnetic circular dichroism

Boyang Liu,[1] Cinthia Piamonteze,[2] Mario Ulises Delgado-Jaime,[1] Ru-Pan Wang,[1] Jakoba Heidler,[2] Jan Dreiser,[2] Rajesh Chopdekar,[2,3] Frithjof Nolting,[2] and Frank M. F. de Groot[1,*]

[1]*Inorganic Chemistry & Catalysis, Debye Institute for Nanomaterials Science, Utrecht University, Universiteitsweg 99, 3584 CG Utrecht, The Netherlands*

[2]*Swiss Light Source, Paul Scherrer Institut, CH-5232 Villigen PSI, Switzerland*

[3]*Department of Materials Science and Engineering, University of California, Davis, California 95616, USA*

(Received 9 March 2017; revised manuscript received 25 July 2017; published 30 August 2017)

The quantitative analysis of 3*d* transition metal $L_{2,3}$ edge x-ray magnetic circular dichroism (XMCD) spectra and the related sum rules are compared for measurements with electron yield and fluorescence yield detection. Multiplet calculations on divalent ions show that fluorescence yield detected sum rule derived expectation values of L_z and S_z show noticeable deviations and detection angle dependence. We show that small deviations of the polarization dependent fluorescent decay values lead to significant deviations in the L_z and S_z sum rule values. Fe and Co experimental XMCD spectra of a supported 10 nm $CoFe_2O_4$ thin film are measured simultaneously by both electron and fluorescence yield. The deviations shown in the experimental data are well explained by the calculations and are shown to mainly depend on the polarization dependent total decay. We conclude that fluorescence yield detected x-ray magnetic circular dichroism is unsuitable for quantitative analysis of the L_z and S_z sum rule values.

DOI: 10.1103/PhysRevB.96.054446

I. INTRODUCTION

XMCD is an experimental tool that probes the difference between x-ray absorption spectra (XAS) obtained with left- and right-circularly polarized x rays. By combining x-ray spectroscopy with magnetometry, XMCD offers the advantage of element specificity to study the electronic and magnetic structure of magnetic materials [1–3]. The optical sum rules [4–6] state that integrals of the XMCD spectrum can be related to ground state expectation values of the spin (S_z) and the orbital (L_z) angular momentum. The determination of S_z and $L_z$turns XMCD into an efficient quantitative analysis tool to study magnetic properties. For 3*d* transition metals, the $L_{2,3}$ edge XMCD spectra have energies in the soft x-ray range with short x-ray penetration lengths of ∼20 nm at the L edge maximum [6,7]. This short x-ray penetration length implies that transmission measurements are difficult and most experiments use electron yield (EY) or fluorescence yield (FY) methods that measure the emitted decay products of the core hole. Due to the short electron escape depth [8,9] EY detection is surface sensitive and, detecting emitted electrons, it is sensitive to the applied magnetic field. FY measurements are not affected by the magnetic field and have larger x-ray escape depths that allow the probe of bulk properties and the detection of buried layers or interfaces. Because the x-ray escape depth is similar to the x-ray penetration depth, FY detection is susceptible to saturation and self-absorption effects in nondilute samples [10,11].

The property that we investigate in this paper is the fact that FYXAS is intrinsically distorted. It turns out to be the case that the FY intensity is not proportional to the absorption coefficient due to the energy-dependent variation in the integrated x-ray emission intensities [12,13]. Deviations of the FYXAS shapes due to the intrinsic variations of fluorescence decay strengths has been demonstrated by Kurian *et al.* [14].

Although the identification of FYXAS to EYXAS (referred to as XAS in the following text) had been disapproved, it is not obvious whether the intrinsic variations of fluorescence decay have large effects on the sum-rule-derived L_z and S_z expectation values. The theoretical analysis by van Veenendaal *et al.* [15] suggested that when the total fluorescence decay is not strongly polarization dependent, only small deviations exist in the L_z and S_z values obtained by FY detection, implying that the sum rules hold for $L_{2,3}$ edges of 3*d* transition metals and $M_{4,5}$ edges of light rare earths ($n < 7$). Nevertheless, arguments were also raised concerning the angular dependence of the sum rule results [16]. In the current work, we revisit this issue from both the theoretical and experimental side. Theoretically, multiplet calculations were used to investigate the spectral difference between XMCD and FYXMCD. The respective sum-rule-derived L_z and S_z values obtained under different detection directions were compared. The calculations were focused on the magnetically most studied 3*d* transition metal elements Mn, Fe, Co, and Ni. Experimentally, Fe and Co XMCD spectra of the $CoFe_2O_4$ thin film were obtained by using both EY and FY methods. Sum rules were applied on the spectra of both elements to examine the expectation values obtained by both yield methods.

II. THEORY AND EXPERIMENT

A. Multiplet calculations

The calculations were performed with the ligand field multiplet approach by using the Cowan-Butler-Thole multiplet code [17–19]. In order to simplify the model and to focus on the essence of the deviations of FY in $L_{2,3}$ XAS and XMCD, charge transfer effects have been neglected, where we note that charge transfer effects are more prominent in covalent systems. In divalent transition metal oxides charge transfer effects are small and the initial state configuration is described by a $2p^6 3d^n$ configuration.

*F.M.F.deGroot@uu.nl

In the $2p$ XAS calculation the dipole transitions from the initial configuration $2p^6 3d^n$ to the final state $2p^5 3d^{n+1}$ configurations were considered. In the calculations of the Mn^{2+}, Fe^{2+}, Co^{2+}, and Ni^{2+} ions, atomic values of the Slater integrals (80% of Hartree-Fock calculated values) and spin-orbit couplings ($L \cdot S_p$ and $L \cdot S_d$) were used. Calculations were performed under the octahedral (O_h) symmetry, using a cubic ligand field splitting (10Dq) of 1.0 eV and a super-exchange field (M) of 10 meV. The XMCD spectrum is defined as the absorption of left circularly polarized (positive helicity, μ_{+1}) x rays minus the absorption of right circularly polarized (negative helicity, μ_{-1}) x rays, where we note that the definition of XMCD is inverted in part of the literature.

Auger decay is dominant and it sets the lifetime of $2p^5 3d^{n+1}$ final states. The lifetime of Auger decay is constant for core-core-core channels. It varies in channels where valence states are involved, but this variation is small over the whole spectrum [12]. The $2p3d$ x-ray emission decay is the dominant radiative channel, where we note that the (energy independent) $2p3s$ decay channels has a relative strength of 10% to 20%. Therefore, the FYXAS and FYXMCD spectra will be calculated from the integral over the complete $2p3d$ x-ray emission channel, which is strongly energy and detection angle dependent.

The $2p3d$ inelastic x-ray scattering process is described by the Kramers-Heisenberg equation [20,21]:

$$F(\Omega,\omega) = \sum_f \left| \sum_n \frac{\langle f|T_2|i\rangle\langle i|T_1|g\rangle}{E_g + \Omega - E_i + i\frac{\Gamma}{2}} \right|^2 \times \delta(E_g + \Omega_i - E_f - \omega), \quad (1)$$

where the g, i, and f represents initial state, intermediate state, and final state, respectively. T_1 and T_2 are the dipole operators of absorption and emission. Ω is the energy of the x-ray excitation and ω is the x-ray emission energy. Γ indicates the intermediate states lifetime. Interference effects are included in the calculation with Γ set to 0.4 eV (full width at half maximum, fwhm). The $2p3d$ RIXS calculations were performed in C_4 symmetry that yield nine combinations of left, right, and z polarized incoming and outgoing x rays. FY XMCD spectra were obtained by considering the different emission directions as [22]:

$$I_q^{\text{normal}} = I_{q0} + \tfrac{1}{2}(I_{q1} + I_{q-1}) \quad (2)$$

$$I_q^{\text{iso}} = I_{q0} + I_{q1} + I_{q-1}. \quad (3)$$

The normal geometry relates to the fluorescence detector at 90 degree horizontal scattering with respect to the magnetic axis. The isotropic signal [15,16] is obtained from the fluorescence signal detection integrated over all angles or with the detector at 54.7 degrees [$\arccos(1/\sqrt{3})$] with respect to the magnetic axis. The calculated transitions were convoluted with Lorentzian and Gaussian functions to account for the lifetime broadening and experimental resolution, respectively.

B. Procedure to obtain the sum-rule-derived values

The sum rules apply to the transition between the $2p$ level and $3d$ level. The integrated $2p3d$ x-ray absorption spectrum over the whole $L_{2,3}$ edge is proportional to the number of $3d$ holes($\langle n_h \rangle$). The absorption coefficient (μ) includes the individual left (μ_{+1}), right (μ_{-1}), and z (μ_0) polarized components as: $\int \mu = \int(\mu_{+1} + \mu_{-1} + \mu_0)$. Under the assumption that the z polarized component is equal to the average of the left and right components, the orbital momentum sum rule is defined as:

$$\langle L_z \rangle = \frac{4}{3}\langle n_h \rangle \frac{\int_{L_3+L_2}(\mu_{+1} - \mu_{-1})}{\int \mu}. \quad (4)$$

The spin sum rule yields an integral for the effective spin momentum, i.e., $\langle SE_z \rangle = \langle S_z \rangle + \frac{7}{2}\langle T_z \rangle$. To simplify the analysis, we assume that the spin-quadrupole coupling $\langle T_z \rangle$ is zero, implying that $\langle S_z \rangle$ equals the effective spin moment $\langle SE_z \rangle$ [23]. The spin sum rule is given as:

$$\langle S_z \rangle = \langle n_h \rangle \frac{\int_{L_3}(\mu_{+1} - \mu_{-1}) - 2\int_{L_2}(\mu_{+1} - \mu_{-1})}{\int \mu}. \quad (5)$$

For the application of the spin sum rule, the core hole spin-orbit coupling must be much larger than the $2p3d$ multiplet effects, yielding well separated L_3 and L_2 edges. Although the L_3 and L_2 edges of $3d$ transition metals appear separated in shape, they are strongly mixed in character due to the large $2p3d$ multiplet effects [23]. The division energy of the L_3 and L_2 edges was chosen to be consistent in both XMCD and FYXMCD spectra that ensures the effective comparison of $\langle S_z \rangle$ values.

C. Sample preparation

The experiments have been performed on a 10 nm (011)-oriented $CoFe_2O_4$ thin film supported on $[Pb(Mg_{1/3}Nb_{2/3})O_3]_{0.68}$-$[PbTiO_3]_{0.32}$ substrate. The film was synthesized via pulsed laser deposition at a substrate temperature of 590 °C in an oxygen ambient of 1×10^{-4} Torr using a KrF excimer laser fluence of 1.3 J/cm^2. The sample was cooled to room temperature in an atmosphere of 1 Torr of oxygen after deposition. SQUID magnetization measurements show that the Curie temperature is above 600 K.

D. X-ray absorption experiments

The sample was measured at room temperature at the X-Treme beamline at the Swiss Light Source [24]. The measurements were carried out with a 30 degree grazing incident x-ray beam along the substrate (100) direction. A 2 Tesla magnetic field was applied along the incident beam direction. The FY detector was set at 90 degree horizontal scattering. The EY and FY XAS spectra with left or right circularly polarized incident x rays were acquired simultaneously.

III. RESULTS

A. Theoretical spectral shapes

Figure 1 shows the calculated XAS and XMCD spectra together with the FY counterparts detected under, respectively, 90° and isotropic scattering geometry. Calculations are shown for Mn^{2+} ($3d^5$), Fe^{2+} ($3d^6$), Co^{2+} ($3d^7$), and Ni^{2+} ($3d^8$) ions. The calculated XAS and XMCD only include the left and right polarized components. The XAS and FYXAS spectra

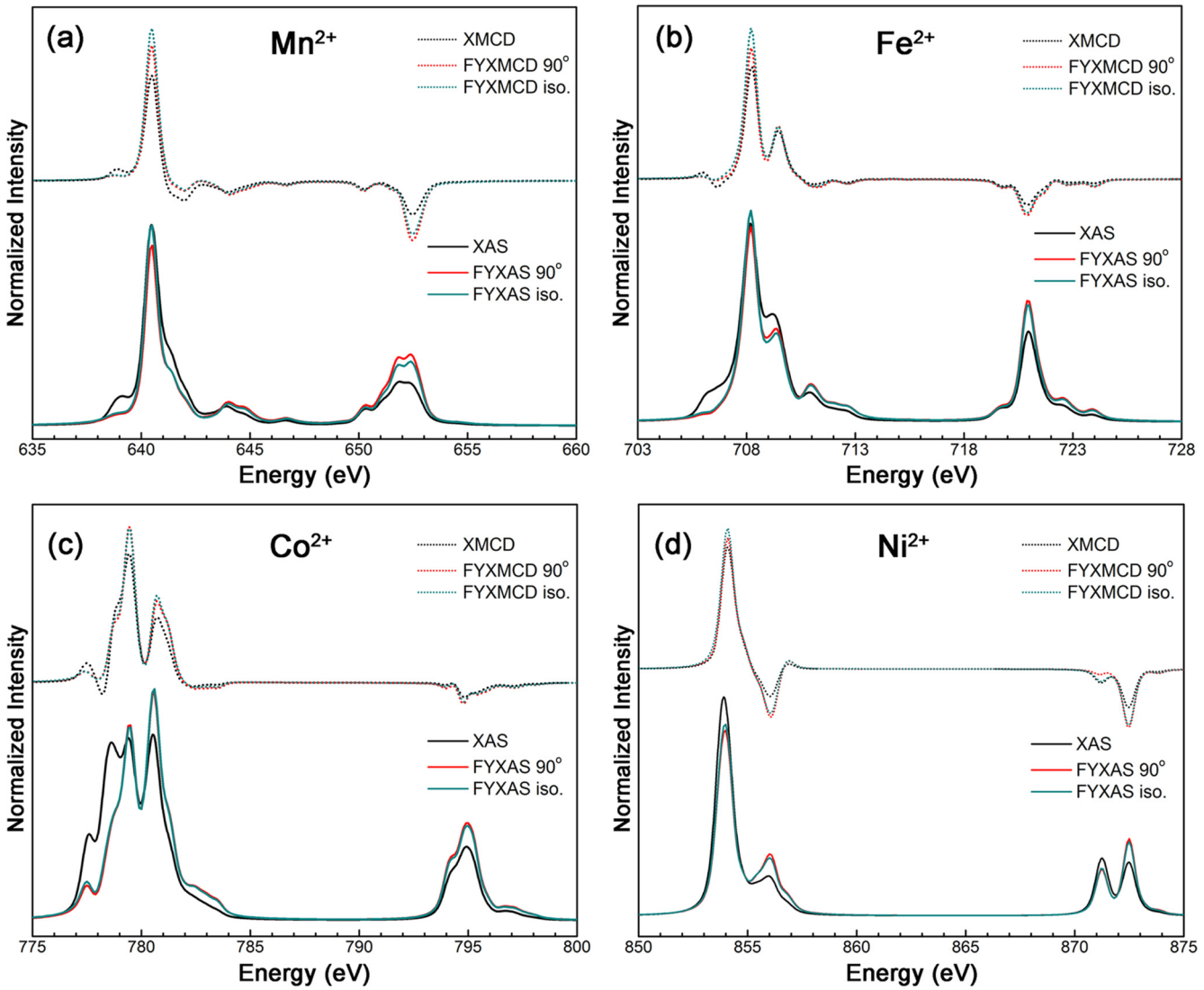

FIG. 1. The calculated $L_{2,3}$ XMCD and FYXMCD (dashed lines), XAS and FYXAS (solid lines) spectra of (a) Mn^{2+}, (b) Fe^{2+}, (c) Co^{2+}, and (d) Ni^{2+} ions. EY spectra are with the black color; FY spectra of 90° and isotropic detection geometries are with red and green colors, respectively. XMCD and FYXMCD spectra are all inverted for plotting.

are normalized to the corresponding integral values, and both XMCD and FYXMCD spectra are shown inverted.

A general trend is observed with the FYXAS giving increased intensity at the higher energy side of the L_3 edge and an increased intensity of the L_2 edge. The observed distortion in FYXAS shape had been explained by the state dependent fluorescence decay ratio [12,14]. The fluorescent decay matrix element was shown to be proportional to the exchange integral G^1_{pd} [15]. The differences between FYXAS spectra under the two geometries are minor. The spectral shape difference between the XMCD and FYXMCD spectra is smaller than the difference between XAS and FYXAS.

B. Theoretical sum rule values

The sum-rule-derived L_z and S_z values from the calculated XMCD and FYXMCD spectra under both scattering geometries are listed in Table I. The deviations indicate the FYXMCD values with respect to the XMCD values, where the values shown in Table I are based on the spectra plotted in Fig. 1.

The Mn^{2+} ($3d^5$) ion in the current calculation is in the high spin ground state $^6A_1$ symmetry, in which the electron occupation can be approximated as $t_{2g}^3 e_g^2$. The orbital momentum is, in first approximation, zero with no effective influence of the valence spin orbit coupling. The sum-rule-derived L_z value from current XMCD calculation is approximately -0.001, i.e., not exactly zero due to minor mixing of excited quartet multiplet states. The sum-rule-derived L_z values from FYXMCD spectra with 90° and isotropic scattering geometries are -0.077 and 0.317, respectively, which strongly deviates from the XMCD result. For the Fe^{2+} ($3d^6$) ion, the sum-rule-derived L_z values from FYXMCD under two detection geometries deviate $\sim\pm 20\%$ from the expectation value obtained from XMCD. The large difference between L_z values obtained by the two fluorescence scattering geometries indicates that sum rule results are dependent on fluorescence detection direction, which is related to the departure from spherical symmetry in the intermediate state [16].

TABLE I. Sum-rule-derived L_z and S_z values obtained from calculated XMCD and FYXMCD (90° and isotropic detections) spectra (Fig. 1) of Mn^{2+}, Fe^{2+}, Co^{2+}, and Ni^{2+} ions. Deviations of L_z and S_z values obtained from FY spectra with respect to that from EY spectra are calculated based on $\frac{\text{FYXMCD}-\text{XMCD}}{\text{XMCD}}\%$. The sum-rule-derived S_z values were calculated by using divisions of the L_3 and the L_2 edges at, respectively, 649 eV, 717 eV, 790 eV, and 862 eV for Mn^{2+}, Fe^{2+}, Co^{2+}, and Ni^{2+} ions.

	XMCD	FYXMCD (90° detection)	*Deviation*[a]	FYXMCD (iso. detection)	*Deviation*[a]
$\langle L_z \rangle$					
Mn^{2+}	−0.001	−0.077		0.317	
Fe^{2+}	0.756	0.621	*−18%*	0.902	*19%*
Co^{2+}	0.909	0.986	*9%*	1.045	*15%*
Ni^{2+}	0.320	0.219	*−32%*	0.293	*−8%*
$\langle S_z \rangle$					
Mn^{2+}	1.664	2.572	*55%*	2.636	*58%*
Fe^{2+}	1.423	1.719	*21%*	1.814	*27%*
Co^{2+}	0.929	1.119	*20%*	1.114	*20%*
Ni^{2+}	0.920	0.954	*4%*	1.061	*15%*

[a]The percentage of the deviation of L_z of Mn^{2+} is large, as the XMCD value is close to zero.

The S_z values obtained from FY spectra deviate more than 50% for Mn^{2+}, between 20% and 30% for Fe^{2+} and Co^{2+} ions, and below 15% for Ni^{2+} ion, where they show little detection geometry dependence. The S_z values are known to be more correct with increasing 3*d* count due to their larger spin-orbit coupling, and we find that the additional error due to FY follows the same trend.

C. The iron $L_{2,3}$ edge of $CoFe_2O_4$ compared with theory

The Fe and the Co $L_{2,3}$ edge XMCD and FYXMCD spectra from the $CoFe_2O_4$ thin film were measured to experimentally determine the spectral differences between the two detection methods. $CoFe_2O_4$ has an inverse spinel structure, in which Co^{2+} occupies the O_h sites and Fe^{3+} is split between the O_h and the tetrahedral (T_d) sites. Previous studies [25] showed that iron in the $CoFe_2O_4$ is distributed over the Fe^{2+} O_h, Fe^{3+} O_h, and Fe^{3+} T_d sites and consequently Co will also contain the Co^{3+} T_d component to balance the charge. The distribution of the cobalt components is correlated with the sample preparation conditions including sample forming temperatures and fast cooling rates, etc. [26]. The Fe^{2+} and Fe^{3+} ions in O_h sites are ferromagnetic and the Fe^{3+} ions in T_d sites are antiferromagnetic. The weights of the Fe components were obtained with a fitting procedure. The upper panel of Fig. 2 shows the experimental Fe $L_{2,3}$ XMCD spectrum together with the calculated result. Both XMCD spectra were normalized to the corresponding XAS integral and the obtained calculated spectrum was scaled to the intensity of the experimental XMCD spectrum at 709.1 eV. This normalization procedure allows a direct comparison between the calculated and experimental spectra. The calculated spectrum disagrees with the experimental data at 712–713 eV, which is caused by the omission of charge transfer effects in the current calculations. In the lower panel of Fig. 2, separate XMCD spectra of Fe^{2+} O_h, Fe^{3+} O_h, and Fe^{3+} T_d components are presented, scaled by their determined presence of, respectively, 12%, 55%, and 33%.

The upper panel of Fig. 3 shows the Fe $L_{2,3}$ edge experimental XMCD and FYXMCD spectra from the $CoFe_2O_4$ thin film, where the dashed lines indicate the respective integrals. The spectra are normalized to their respective XAS integral. Because the XMCD and FYXMCD spectra are normalized to their respective XAS and FYXAS signals, the integrals are proportional to the L_z values. Note that the integral of the FYXMCD spectrum has an opposite sign. The sum-rule-derived S_z values from the experimental XMCD and FYXMCD are, respectively, −0.093 and −0.044, which were calculated by separating the L_3 and L_2 edges at 718 eV and considering the number of holes of average three Fe components as 4.88. The large experimental deviations in the L_z and S_z values confirms that FY is unsuitable for quantitative XMCD analysis.

The lower panel of Fig. 3 shows the calculated Fe spectra that are compared with the experimental results in the upper panel. The theoretical spectra were plotted after the same normalization procedure as was used in Fig. 2. The calculation

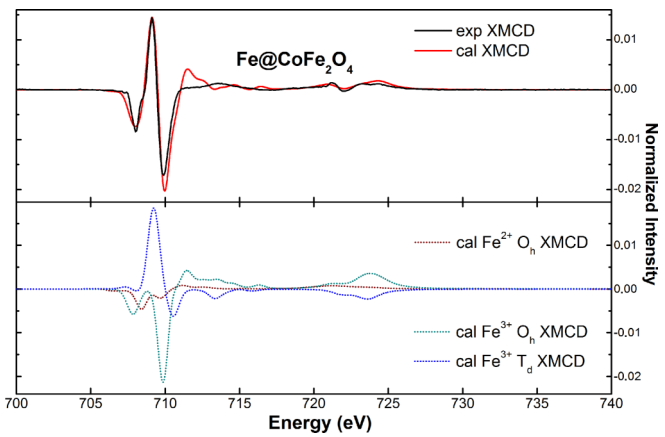

FIG. 2. Upper panel: Experimental (black line) and calculated (red line) Fe $L_{2,3}$ XMCD spectra of the $CoFe_2O_4$ thin film. Lower panel: the calculated XMCD spectra of Fe^{2+} O_h (wine red dots), Fe^{3+} O_h (green dots), and Fe^{3+} T_d (blue dots) components. The calculated spectra include contributions of the ground state and all Boltzmann distributed excited states at 300 K.

TABLE II. Ligand field multiplet parameters used for calculating Fe spectra of the $CoFe_2O_4$ thin films. All values are given in eV. The bottom panel of the table gives the reduction of the Slater integrals (F^2_{dd}, F^4_{dd}, F^2_{pd}, G^1_{pd} and G^3_{pd}) with respect to their atomic values, as derived from the fitting procedure. The value for the exchange field in all calculations is 41 meV.

Parameter (eV)	F^2_{dd}	F^4_{dd}	F^2_{pd}	G^1_{pd}	G^3_{pd}	$L \cdot S_p$	$L \cdot S_d$	10Dq
Fe^{2+} O_h								
Initial state (EY&FY)/final state (FY)	8.097	5.032					0.025	1.240
Intermediate state (FY)/final state (EY)	8.697	5.410	4.942	3.643	2.070	8.200	0.033	1.240
Fe^{3+} O_h								
Initial state (EY&FY)/final state (FY)	8.843	5.533					0.029	1.780
Intermediate state (FY)/final state (EY)	9.413	5.891	5.461	4.081	2.322	8.199	0.036	1.780
Fe^{3+} T_d								
Initial state (EY&FY)/final state (FY)	8.926	5.585					0.029	−0.650
Intermediate state (FY)/final state (EY)	9.501	5.946	5.501	4.145	2.358	8.199	0.036	−0.650
Parameter (atomic value %)	F^2_{dd}	F^4_{dd}	F^2_{pd}	G^1_{pd}	G^3_{pd}	$L \cdot S_p$	$L \cdot S_d$	
Fe^{2+} O_h	92.3	92.3	90.9	91.0	91.0	100	49.0	
Fe^{3+} O_h	91.8	91.8	91.7	91.7	91.7	100	49.0	
Fe^{3+} T_d	92.7	92.7	92.4	93.1	93.1	100	49.0	

parameters are indicated in Table II. In the FY calculations for the Fe^{2+} O_h component, the lowest five states were included, using a Boltzmann distribution. Together they account for ∼96% of the total room temperature populated states. The integrals of the calculated XMCD and FYXMCD spectra are both in agreement with their experimental counterparts, where in both theory and experiment an inversion of the sign if observed. Note that sharp L_2 edge in the calculated FYXMCD spectrum is due to the too small lifetime broadening used in the calculation. This does not influence the integrated values. We conclude that the sum-rule-derived L_z values obtained from the calculation shows the same deviations as seen in the experimental data. This proves that the effects of the intrinsic fluorescence decay variations modify the expectation values obtained by FY detection. The S_z values extracted from the calculation are, respectively, the −0.115 (XMCD) and −0.148 (FYXMCD). These values differ from those obtained by the experiments. This is likely due to the complications in the spin sum rule [23]. More details on this issue will be given in the discussion below.

D. The cobalt $L_{2,3}$ edge of $CoFe_2O_4$ compared with theory

Figure 4 shows the comparison of the experimental and calculated Co $L_{2,3}$ XMCD spectra. Both spectra present are normalized to their corresponding XAS integrals and the calculated result was further scaled to the intensity of experimental data at 779 eV. The calculation parameters are listed in Table III. The ground state of the Co^{2+} (d^7) ion has $^4T_1$ symmetry. All temperature populated states were included based on the Boltzmann distribution. The experimental spectrum is well reproduced by the calculation, which confirms that the sample contains Co^{2+} O_h.

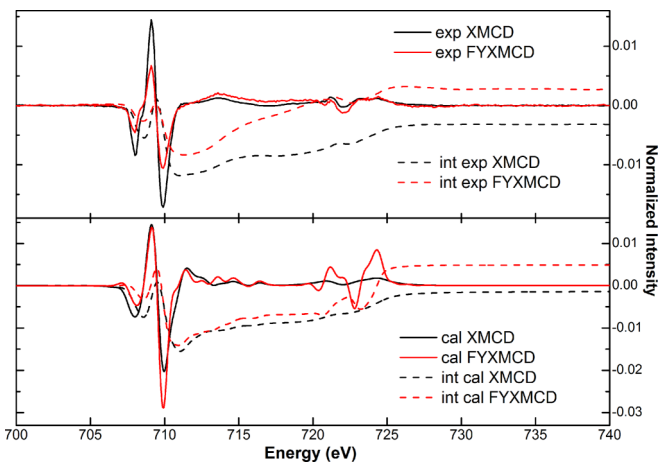

FIG. 3. Fe $L_{2,3}$ XMCD (black line), (FY)XMCD (red line) spectra, and the corresponding integrals (int, dashed lines). Upper panel: experimental results from the $CoFe_2O_4$ thin film. Lower panel: calculation results.

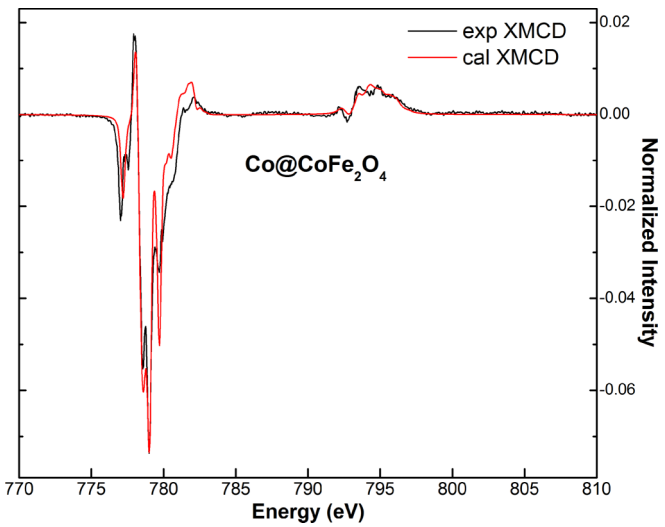

FIG. 4. Experimental (black line) Co $L_{2,3}$ XMCD spectrum of the $CoFe_2O_4$ thin film and the corresponding calculation result (red line).

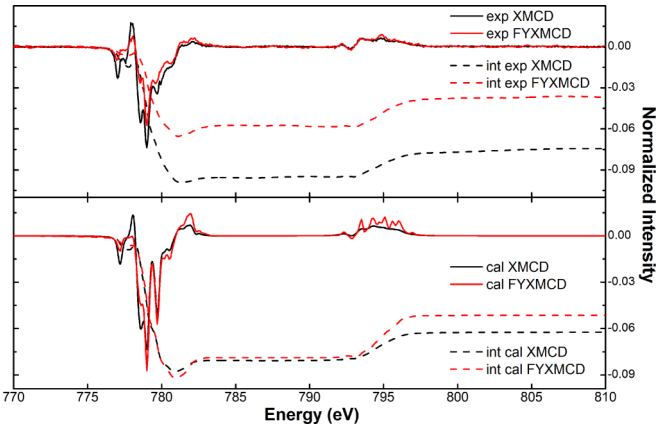

FIG. 5. Co $L_{2,3}$ XMCD (black line), (FY)XMCD (red line) spectra, and the corresponding integrals (int, dashed lines). Upper panel: experimental results from the $CoFe_2O_4$ thin film. Lower panel: calculation results.

Figure 5 shows the experimental (upper panel) and corresponding calculated (lower panel) Co XMCD and FYXMCD spectra together with the integrals. The deviation of sum-rule-derived Co L_z values from experimental data is reflected by the difference of integral values. The difference is smaller in the calculation, but the same trend is observed. The sum-rule-derived L_z values from the calculated XMCD and FYXMCD spectra are, respectively, -0.25 and -0.21, giving a $\sim -18\%$ deviation for the value from FY. For the S_z, the sum-rule-derived values from the experimental data are -0.148 (XMCD) and -0.106 (FY). The S_z values obtained from the calculated spectra show a $\sim 14\%$ deviation. We note that S_z values from current calculation results are not directly comparable to that obtained from experiments by using the spin sum rule [23].

IV. DISCUSSION

A. Polarization dependence of the integrated x-ray emission

In Ref. [15], van Veenendaal *et al.* showed that $I_q^{fluor} = I_q^{XAS}\langle V^\Gamma\rangle_q$, where the I_q^{fluor} and I_q^{XAS} are, respectively, the integrated intensity of fluorescence and XAS with the polarization of q (0 and ± 1), and $\langle V^\Gamma\rangle_q$ is defined as the *total* decay. Based on this equation, the requirement for using FYXMCD as a quantitative tool is that the $\langle V^\Gamma\rangle_q$ has no strong polarization dependence. The $\langle V^\Gamma\rangle_q$ values of Mn^{2+}, Fe^{2+}, Co^{2+}, and Ni^{2+} ions under two detection geometries were calculated to correlate with deviations of the sum-rule-derived values from

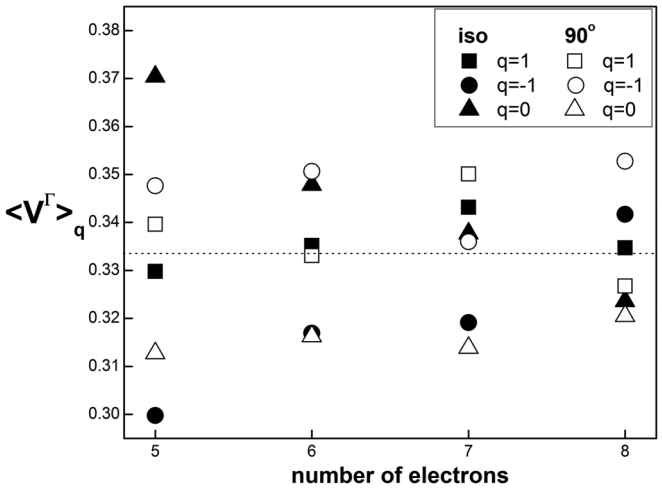

FIG. 6. The calculated total decay $\langle V^\Gamma\rangle_q$ for Mn^{2+}, Fe^{2+}, Co^{2+}, and Ni^{2+} ions with the $3d$ electron occupation from 5 to 8. Solid and hollow symbols correspond to the FY detection geometry of isotropic and 90°, respectively. Components of different polarizations are represented by square ($q = 1$), circle ($q = -1$), and triangle ($q = 0$). The dotted straight line represents the value of $\frac{1}{3}$.

fluorescence detections. The $\langle V^\Gamma\rangle_q$ values shown in Fig. 6 are after the normalization of $\sum_q \langle V^\Gamma\rangle_q = 1$. When all three $\langle V^\Gamma\rangle_q$ equal $\frac{1}{3}$ (the value shown as the dotted line in Fig. 6), the fluorescence decay is polarization independent. It is seen from Fig. 6 that deviations of total decay values from $\frac{1}{3}$ are relatively small, similar to the results shown in Ref. [15]. A relatively large deviation of the total decay happens for the Mn^{2+} ion under isotropic detection geometry. This may partly explain the large deviations found in its L_z and S_z values as shown in Table I. One qualitative relationship between the total decay and the deviation of L_z values found is when $\langle V^\Gamma\rangle_1$ (square signs in Fig. 6) is larger than $\langle V^\Gamma\rangle_{-1}$ (circle signs in Fig. 6), the L_z value obtained by FY detection is larger than that by EY detection and *vice versa*. Furthermore, although not linearly, the larger difference between $\langle V^\Gamma\rangle_1$ and $\langle V^\Gamma\rangle_{-1}$, the larger deviation of FY L_z values are shown. However, the full quantitative relationship between the differences of total decay values ($q = 1$ or $q = -1$) and the deviation of L_z and S_z values obtained by FY is more complex. For example, under the isotropic detection, the deviation for the L_z value of Fe^{2+} ion is larger than that of Co^{2+} ion but the deviation for the total decay value of Fe^{2+} ion is smaller. In the case of S_z values, the calculated deviations are even more difficult to be correlated with that for total decay values. Nevertheless, the comparison

TABLE III. Ligand field multiplet parameters used for calculating Co spectra of the $CoFe_2O_4$ thin films. All values are given in eV. The bottom panel of the table gives the reduction of the Slater integrals with respect to their atomic values. The exchange field exchange in all calculations is 41 meV.

Parameter (eV)	F^2_{dd}	F^4_{dd}	F^2_{pd}	G^1_{pd}	G^3_{pd}	$L \cdot S_p$	$L \cdot S_d$	10Dq
Initial state (EY&FY)/final state (FY)	9.052	6.416					0.041	1.070
Intermediate state (FY)/final state (EY)	9.669	7.708	6.244	4.911	3.069	9.748	0.051	1.070
Parameter (atomic value %)	F^2_{dd}	F^4_{dd}	F^2_{pd}	G^1_{pd}	G^3_{pd}	$L \cdot S_p$	$L \cdot S_d$	
	78	89	86	91	100	100	62	

of two deviations indicates that even for fluorescence with small deviated total decay values from $\frac{1}{3}$, or equivalently, with weak polarization dependent total decay $\langle V^{\Gamma}\rangle_q$, may still lead to the large error in the sum-rule-derived L_z or S_z values.

B. Errors in the sum-rule derived S_z value

As discussed above we have added another factor that causes deviations between the sum-rule derived S_z value and the actual value. Previous studies have indicated that two important factors are (1) the value of T_z and (2) the multiplet-induced mixing of the L_3 and L_2 edges [23]. These two factors play a role independent of the detection method. In this paper we added a third intrinsic factor in the form of the difference in the energy-dependent FY decay for left and right polarized x rays. As shown above this effect can be significant and it adds to the two other effects discussed above. It only applies to FY detected spectra of the $L_{2,3}$ edges of $3d$ transition metal systems.

C. Relative shifts in the iron L edge spectra

Important fitting parameters in the calculation of the experimental spectral shape are the relative shifts of the three iron components. In the case of binary Fe^{2+} and Fe^{3+} oxides and complexes, the shift between Fe^{2+} and Fe^{3+} is approximately 1.5 eV [27]. In $CoFe_2O_4$ the octahedral iron sites are coupled by hopping and as such the iron sites can be time averaged as $Fe^{2.5+}$. This implies that the sites are much more similar in Fe-O distances (compared with binary oxides), which in turn implies that the shift is reduced. The fitting procedure finds that the shift is reduced to 0.7 eV, with Fe^{2+} O_h at 711.3 and Fe^{3+} O_h at 712.0, with the Fe^{3+} T_d position at 711.8 eV. The ground state of Fe^{2+} O_h, Fe^{3+} O_h, and Fe^{3+} T_d ions are, respectively, the $^5T_2$, $^6A_1$, and $^6A_1$ symmetries.

D. Applicability of the results for covalent and metallic systems

In general divalent ions have a $2p3d$ RIXS spectrum that is for more than 90% determined by the resonant $2p3d$ channels. Trivalent ions have stronger charge transfer and fluorescence effects, but note that Fe^{3+} is still dominated by the distorted FY signal as is evident from experimental data in this paper and other published data [11]. Because fluorescence channels do not involve excitations to localized $3d$ states, it can be assumed that the fluorescence will have no angular dependence. The absence of angular dependence implies that the FY signal will be a mixture of two components: (1) the angular dependent FY signal as calculated in the paper and (2) the nondistorted XAS signal. This implies that the FYXAS and FYXMCD spectra of covalent and metallic systems will be much closer to undistorted XAS and XMCD. It is important to investigate this further in future studies, in particular regarding possible angular dependent fluorescence for metal spectra. In addition it is possible to measure undistorted FY spectra by measuring the $2p3d$ FY signal or, in appropriate systems, the inverse partial fluorescence yield [28].

V. CONCLUDING REMARKS

We have analyzed the differences between the sum-rule-derived expectation values between XMCD and FYXMCD for Mn^{2+}, Fe^{2+}, Co^{2+}, and Ni^{2+} ions. The theoretical FYXMCD spectra are indeed from the XMCD spectra and in addition they show detection angle dependent shapes. The differences in the spectral shape correlate to intrinsic variations of the intermediate states fluorescence decay strengths. This variation of fluorescence decay strengths also causes deviations in the sum-rule L_z and S_z values obtained by FY, which are also angular dependent. Mn^{2+} ion shows the largest deviation in both L_z and S_z values. The deviations generally decrease with the increase of $3d$ electron occupation.

The deviations in the sum rule can be qualitatively correlated to the total decay $\langle V^{\Gamma}\rangle_q$ of each ion, but we did not find a direct quantitative relationship. The small deviations of $\langle V^{\Gamma}\rangle_q$ values from $\frac{1}{3}$ indicate that the weak polarization dependent total decay does not necessarily imply reliable quantitative FYXMCD.

The Fe and Co $L_{2,3}$ edge XMCD spectra of the $CoFe_2O_4$ thin film measured by both EY and FY are studied. The experimental differences of the EY- and FY-XMCD spectral shapes are reproduced by the calculations, including the resulting difference in the L_z and S_z values. We conclude that, although FY detection shows several advantages over the EY detection, care should be taken by the observed spectral shapes that do not identify with XAS and XMCD spectral shapes. In addition, the sum rule values show intrinsic quantitative information obtained by FY as intrinsic deviations are difficult to be ruled out.

ACKNOWLEDGMENTS

This work was financially supported by the China Scholarship Council and the ERC advanced Grant XRAYonACTIVE, No. 340279.

[1] T. Funk, P. Kennepohl, A. J. Di Bilio, W. A. Wehbi, A. T. Young, S. Friedrich, E. Arenholz, H. B. Gray, and S. P. Cramer, J. Am. Chem. Soc. **126**, 5859 (2004).

[2] T. Funk, W. W. Gu, S. Friedrich, H. X. Wang, S. Gencic, D. A. Grahame, and S. P. Cramer, J. Am. Chem. Soc. **126**, 88 (2004).

[3] M. Mizumaki, K. Yano, I. Umehara, F. Ishikawa, K. Sato, A. Koizumi, N. Sakai, and T. Muro, Phys. Rev. B **67**, 132404 (2003).

[4] B. T. Thole, P. Carra, F. Sette, and G. van der Laan, Phys. Rev. Lett. **68**, 1943 (1992).

[5] P. Carra, B. T. Thole, M. Altarelli, and X. D. Wang, Phys. Rev. Lett. **70**, 694 (1993).

[6] C. T. Chen, Y. U. Idzerda, H. J. Lin, N. V. Smith, G. Meigs, E. Chaban, G. H. Ho, E. Pellegrin, and F. Sette, Phys. Rev. Lett. **75**, 152 (1995).

[7] B. T. Thole, G. van der Laan, J. C. Fuggle, G. A. Sawatzky, R. C. Karnatak, and J. M. Esteva, Phys. Rev. B **32**, 5107 (1985).

[8] J. Vogel and M. Sacchi, J. Electron Spectrosc. Relat. Phenom. **67**, 181 (1994).
[9] R. Nakajima, J. Stohr, and Y. U. Idzerda, Phys. Rev. B **59**, 6421 (1999).
[10] S. Eisebitt, T. Boske, J. E. Rubensson, and W. Eberhardt, Phys. Rev. B **47**, 14103 (1993).
[11] F. M. F. de Groot, Nat. Chem. **4**, 766 (2012).
[12] F. M. F. de Groot, M. A. Arrio, P. Sainctavit, C. Cartier, and C. T. Chen, Solid State Commun. **92**, 991 (1994).
[13] M. Pompa, A. M. Flank, P. Lagarde, J. C. Rife, I. Stekhin, M. Nakazawa, H. Ogasawara, and A. Kotani, Phys. Rev. B **56**, 2267 (1997).
[14] R. Kurian, K. Kunnus, P. Wernet, S. M. Butorin, P. Glatzel, and F. M. F. de Groot, J. Phys.: Condens. Matter **24**, 452201 (2012).
[15] M. van Veenendaal, J. B. Goedkoop, and B. T. Thole, Phys. Rev. Lett. **77**, 1508 (1996).
[16] J. B. Goedkoop, N. B. Brookes, M. van Veenendaal, and B. T. Thole, J. Electron Spectrosc. Relat. Phenom. **86**, 143 (1997).
[17] R. D. Cowan, J. Opt. Soc. Am. **58**, 808 (1968).
[18] R. D. Cowan, in *The Theory to Atomic Structure and Spectra* (University of California Press, Berkeley, CA, 1981).
[19] B. T. Thole, G. van der Laan, and P. H. Butler, Chem. Phys. Lett. **149**, 295 (1988).
[20] H. A. Kramers and W. Heisenberg, Z. Phys. **1**, 681 (1925).
[21] A. Kotani and S. Shin, Rev. Mod. Phys. **73**, 203 (2001).
[22] B. T. Thole, G. van der Laan, and M. Fabrizio, Phys. Rev. B **50**, 11466 (1994).
[23] C. Piamonteze, P. Miedema, and F. M. F. de Groot, Phys. Rev. B **80**, 184410 (2009).
[24] C. Piamonteze, U. Flechsig, S. Rusponi, J. Dreiser, J. Heidler, M. Schmidt, R. Wetter, M. Calvi, T. Schmidt, H. Pruchova, J. Krempasky, C. Quitmann, H. Brune, and F. Nolting, J. Synchrot. Radiat. **19**, 661 (2012).
[25] R. A. D. Pattrick, G. van der Laan, C. M. B. Henderson, P. Kuiper, E. Dudzik, and D. J. Vaughan, Eur. J. Mineral. **14**, 1095 (2002).
[26] Y. Waseda, K. Shinoda, and K. Sugiyama, Z. Naturforsch., A: Phys. Sci. **50a**, 1199 (1995).
[27] F. M. F. de Groot, P. Glatzel, U. Bergmann, P. A. van Aken, R. A. Barrea, S. Klemme, M. Hävecker, A. Knop-Gericke, W. M. Heijboer, and B. M. Weckhuysen, J. Phys. Chem. B **109**, 20751 (2005).
[28] A. J. Achkar, T. Z. Regier, H. Wadati, Y. J. Kim, H. Zhang, and D. G. Hawthorn, Phys. Rev. B **83**, 081106(R) (2011).